JOURNAL OF GEOPHYSICAL RESEARCH, VOL. 113, C09021, doi:10.1029/2008JC004776, 2008

Radon and radium isotope assessment of submarine groundwater discharge in the Yellow River delta, China

Richard N. Peterson,[1] William C. Burnett,[1] Makoto Taniguchi,[2] Jianyao Chen,[3] Isaac R. Santos,[1] and Tomotoshi Ishitobi[2]

Received 15 February 2008; revised 12 June 2008; accepted 7 July 2008; published 11 September 2008.

[1] Naturally occurring chemical tracers were used to assess the magnitude of submarine groundwater discharge (SGD) during two different sampling periods at a coastal site south of the Yellow River delta, China. We used salinity and pH as indicators of the terrestrial and recirculated seawater components of discharging groundwater and radium isotopes to quantify offshore transport rates. We then used an hourly time series of multiple radium isotopes (^{224}Ra, ^{223}Ra, and ^{226}Ra) to quantify SGD rates and also used ^{222}Rn and seepage meters to independently quantify SGD rates as a comparison to the radium results. Offshore transport rates were found to range from 3.3 to 4.7 cm s^{-1}. Modeled time series radium activities indicated average SGD rates ranging from 4.5 to 13.9 cm d^{-1} in September 2006 and from 5.2 to 11.8 cm d^{-1} in July 2007. Temporal trends associated with the radium approach agree with SGD patterns revealed by automated seepage meters deployed nearby, but the absolute fluxes are about 70% lower than those determined by the seepage meters. Modeled SGD rates based on ^{222}Rn (mean = 13.8 cm d^{-1} in 2006 and 8.4 cm d^{-1} in 2007) agree with those determined by the radium analysis. Differences in derived SGD rates between the different radium isotopes (^{226}Ra highest; ^{224}Ra lowest) are likely results of uncertainties in the background activities and our limited selection of appropriate groundwater/pore water end-member values. Scaling our results to the entire Yellow River delta, we find SGD fluxes (and corresponding nitrate fluxes) 2–3 times that of the Yellow River.

Citation: Peterson, R. N., W. C. Burnett, M. Taniguchi, J. Chen, I. R. Santos, and T. Ishitobi (2008), Radon and radium isotope assessment of submarine groundwater discharge in the Yellow River delta, China, *J. Geophys. Res.*, *113*, C09021, doi:10.1029/2008JC004776.

1. Introduction

[2] Submarine groundwater discharge (SGD) is now regarded as an important pathway that transports dissolved substances from subseabed fluids to the coastal ocean. Being both spatially and temporally variable, SGD is very difficult to measure and therefore its relative importance in coastal ocean chemical budgets is often unknown [*Burnett et al.*, 2006a]. Nonetheless, nutrient fluxes via SGD have been shown to rival those from rivers in some locations [*Slomp and Van Cappellen*, 2004; *Kim et al.*, 2005; *Swarzenski et al.*, 2007a]. Providing an additional nutrient source to the coastal ocean can often be beneficial to the coastal ecology [e.g., *Santos et al.*, 2008], but effects from SGD can also be harmful in areas where terrestrial groundwaters are contaminated from anthropogenic sources [*Hu et al.*, 2006].

[3] By definition, SGD includes all water moving across the sediment-water interface and into the overlying water column, regardless of composition or driving force [*Burnett et al.*, 2003a]. This designation includes both fresh, terrestrial groundwater and saline, recirculated seawater. The hydraulic gradient is the main driving force that results in fresh, terrestrial aquifer waters discharging at the coastline. Driving forces controlling recirculated seawater include tidal pumping, wave setup, and convective circulation caused by subterranean aquifer density differences [*Michael et al.*, 2005; *Charette*, 2007].

[4] The Yellow River delta is an area where these driving forces can interact uniquely because of some unusual geological characteristics. The high rate of sediment supply from the Yellow River results in an annual progradation of the delta into the Bohai Sea by 20–25 km^2 [*Chen et al.*, 2007]. This growth creates large expanses of low-lying land extending into the Bohai Sea each year. The result is a dampening of the hydraulic gradient between the land and ocean, thereby increasing the relative influence of marine effects as a driving force. This high sediment supply, however, has also created a perched riverbed in the lower reaches of the river, so the Yellow River lies up to 11 m

[1]Department of Oceanography, Florida State University, Tallahassee, Florida, USA.
[2]Research Institute for Humanity and Nature, Kyoto, Japan.
[3]School of Geography Sciences and Planning, Sun Yat-sen University, Guangzhou, China.

0148-0227/08/2008JC004776$09.00

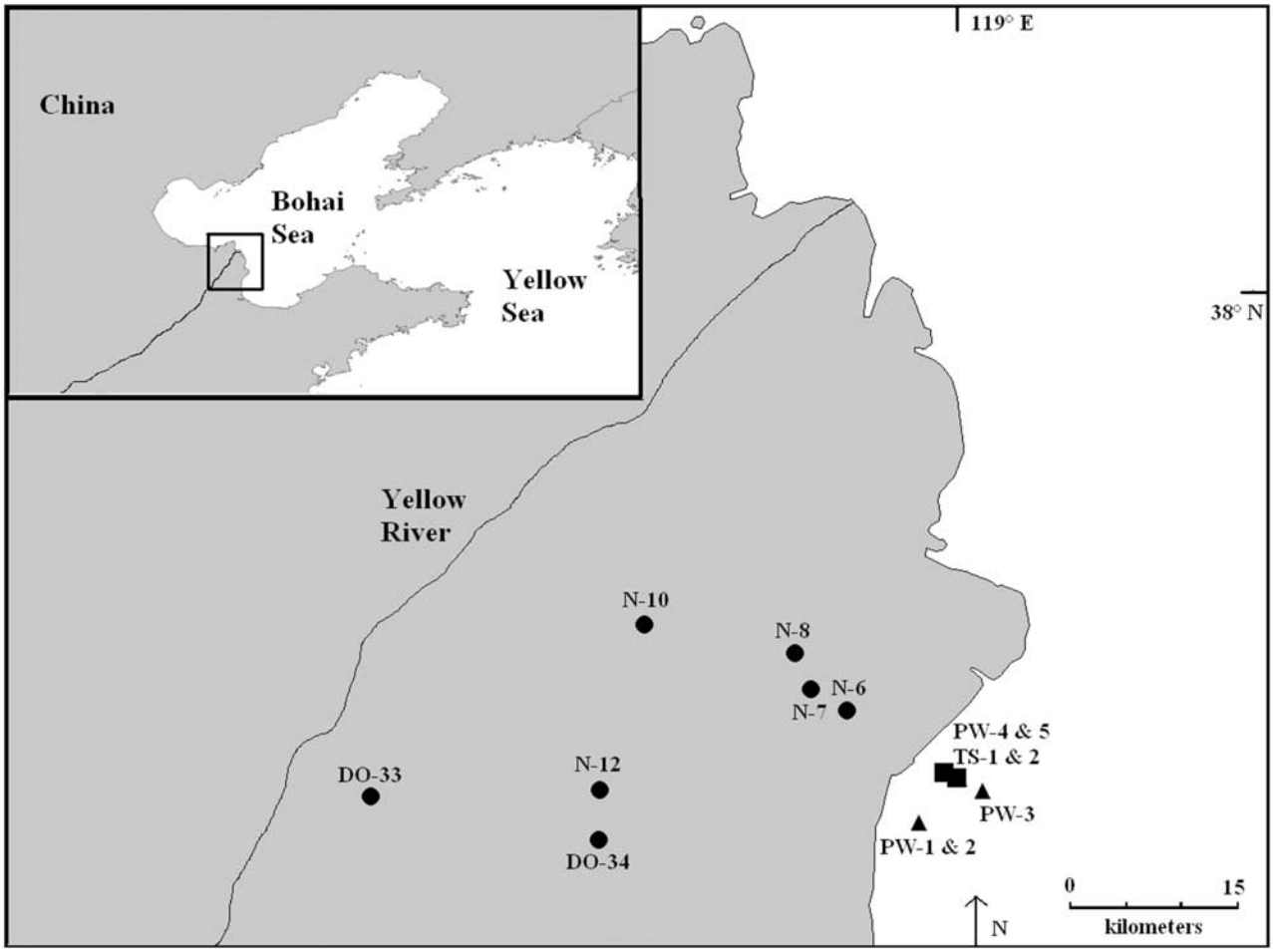

Figure 1. Map showing the Yellow River delta, monitoring wells (circles), and the SGD study site.

above its surroundings. This effect creates the potential for the river to recharge the groundwater, enhancing the hydraulic gradient between the river and the coast [*Yu*, 2006].

[5] The Yellow River delta is a location where SGD can potentially introduce contaminated groundwater to the coastal ocean. As a result of China's growing population, more people are inhabiting the delta than ever before and are contributing to groundwater contamination, mainly through agricultural practices and sewage disposal. The groundwater environment around the delta contains elevated nitrate levels (concentrations up to 3.8 mmol), mainly in shallow aquifers [*Chen et al.*, 2007]. These nitrate-rich zones often coincide with agricultural land use patterns and concentrated population centers. *Zhang et al.* [2004] determined that within the last 40 years, DIN concentrations have increased tenfold, coincident with reductions in phosphorus (50–60%) and silica (75%) in the central Bohai Sea. This trend has led to portions of the Bohai Sea shifting to a phosphate-limited ecosystem. The source of the excess nitrogen, however, remains unknown.

[6] One potential source of this nitrogen could be SGD. Because *Chen et al.* [2007] found excessively high concentrations of nitrate in contaminated groundwater, even a relatively small volumetric flux of SGD could provide a significant input of nitrate to the coastal ocean. Once these nutrients are introduced to the coastal zone via SGD, they must be transported offshore to the central Bohai Sea to contribute to the increasing nitrogen concentrations. In addition to quantifying SGD rates, knowledge of dissolved component transport rates in this region is thus an important factor for determining whether SGD can be a significant source of these nutrients on a regional basis.

[7] *Taniguchi et al.* [2008] used automated heat-type benthic seepage meters [*Taniguchi and Iwakawa*, 2001] to measure SGD in a down-gradient area of the delta approximately 40 km south of the Yellow River estuary (Figure 1). Combining the results from the seepage meters with conductivity (salinity) measured inside the chambers allows for the separation of fresh SGD from total SGD. They found that fresh groundwater fluxes are between 1 and 5% of total flow, and integrating their results over the estimated zone of discharge in the delta yielded freshwater SGD flow estimates that ranged from 4.5 to 7.0% of the Yellow River discharge.

[8] The goals of the work presented here are to use naturally occurring geochemical tracers (e.g., radium isotopes, ^{222}Rn, salinity, pH) to examine patterns and fluxes of SGD in the same area studied by *Taniguchi et al.* [2008]. This paper represents one of the first to use a

24-hour high-resolution time series of multiple radium isotopes in order to quantify SGD rates. *Beck et al.* [2007, 2008] have made similar attempts, but only over ~6-hour intervals. We also use parallel ^{222}Rn and benthic seepage meter measurements to provide an independent comparison of these fluxes.

[9] Chemical tracers measured in the water column integrate the SGD signal over much larger spatial scales than individual benthic chambers, and are thus an appropriate way to handle the large spatial variability inherent in groundwater discharge patterns. In addition, horizontal offshore transects of radium isotopes allow us to quantify the transport rates of the discharged groundwater offshore. Radon and radium isotopes have been shown to be effective tracers of SGD because they are concentrated in groundwater relative to surface water, and the decay rates of the ^{222}Rn and the short-lived radium isotopes are on the same temporal scale as the processes in question [*Burnett and Dulaiova*, 2003; *Kim et al.*, 2005; *Dulaiova et al.*, 2006; *Burnett et al.*, 2008; *Swarzenski et al.*, 2007a]. We use three radium isotopes in this study, with half-lives that cover a large temporal range: ^{224}Ra ($T_{1/2}$: 3.6 days); ^{223}Ra ($T_{1/2}$: 11.3 days); and ^{226}Ra ($T_{1/2}$: 1600 years). In freshwater, radium will be found mostly adsorbed onto the surface of particles, but once introduced to saltwater, ion exchange processes displace the radium off particles and into solution [*Li and Chan*, 1979; *Nozaki et al.*, 2001].

2. Methods

2.1. Measurements

[10] Samples were collected in September 2006 and July 2007 from a coastal site located 40 km south of the Yellow River mouth (small square on the west side of Laizhou Bay, Figure 1) in an area toward which groundwater contours indicate subsurface flow should occur [*Chen et al.*, 2007; *Taniguchi et al.*, 2008]. In September 2006, we collected a continuous 25-hour time series (TS-1; 1 km offshore; average depth: 1.4 m) of radium isotopes, ^{222}Rn, pH, and conductivity. During the July 2007 sampling, these tracers were measured in both a 23-hour time series (TS-2; 2 km offshore; average depth: 1.7 m) and a 12 km shore-normal transect.

[11] Radium isotopes were collected according to the methods established by *Moore and Reid* [1973]. Large volume samples (~100 L) were pumped slowly (1 L min^{-1}) through columns containing acrylic fibers impregnated with manganese dioxide. This Mn-fiber quantitatively sorbs the dissolved radium from the water. These fibers were then washed thoroughly to remove all particles and counted for the short-lived radium isotopes via a delayed coincidence counting system [*Moore and Arnold*, 1996]. ^{226}Ra was counted by either gamma spectrometry [*Dulaiova and Burnett*, 2004] or by measuring ^{222}Rn and its daughters after sealing the fiber in airtight columns to allow for ingrowth. These columns were later mounted to a radon emanation line or a commercially available radon-in-air monitor (RAD7, Durridge Co.) to measure ^{222}Rn as a proxy for the ^{226}Ra [*Kim et al.*, 2001]. All samples from TS-1 were counted by gamma spectrometry, while the samples from July 2007 were analyzed for ^{226}Ra using the ingrowth method. Cross-calibration shows that the methods agree within 20%.

[12] ^{222}Rn in water was measured continuously in the field using a modified RAD7 radon-in-air monitor [*Burnett et al.*, 2001]. Surface water (~0.5 m below the surface) was pumped to an air/water equilibrium exchanger system. In this system, the headspace air is circulated to the RAD7 for analysis of ^{222}Rn activity in the air, and recycled back to the exchanger, creating a closed air loop. Applying a temperature-dependent solubility coefficient for ^{222}Rn, we can convert from measured radon in air to the corresponding value in the water. Each data point attained represents an integrated value over 30 to 60 min, depending upon the desired measurement uncertainty.

[13] Groundwater samples for ^{222}Rn and radium were collected on land using a peristaltic pump from boreholes around the delta, and pore water samples from offshore (~50 cm below the sediment-water interface) were collected from a push-point piezometer [*Charette and Allen*, 2006]. Groundwater and pore water samples for radon were measured using a RAD-H_2O system that uses the internal pump of the RAD7 to sparge radon from a 250 mL volume and circulate it to the counter for measurement. The pH and electrical conductivity were measured using a handheld YSI Model 85 probe.

2.2. Transport Rate Model

[14] *Moore* [2000] described a method of using radium isotope activity ratios (AR) to determine the apparent radium age of water masses. The ages represent the relative time that has elapsed since the radium first entered the system. They are based on the exponential decay of the short-lived radioisotopes from their original input signature. If radium is input to the coastal ocean with a constant short-lived to long-lived AR over time, and no additional sources of radium exist, we can examine the difference between the initial activity ratio (AR_i) and a measured ratio (AR_{obs}) to calculate the apparent radium age (t):

$$t = Ln\left(\frac{AR_i}{AR_{obs}}\right) * \frac{1}{\lambda_{224} - \lambda_{226}} \quad (1)$$

where λ_{224} and λ_{226} represent the decay constants of the short-lived radium isotope (e.g., ^{224}Ra) and that of the longer-lived isotope (e.g., ^{226}Ra), respectively. Defining the ARs as the activity of a short-lived isotope to that of a longer-lived isotope dictates that they always decrease with time.

[15] The relative differences between the radium ages across a transect should indicate the actual mixing times required to distribute the observed isotope ratios. Therefore, plotting the apparent radium ages against their distance from shore (assuming the source is near the shoreline) can yield an estimate of the offshore linear transport rate of radium [*Moore and Krest*, 2004; R. Peterson et al., Determination of transport rates in the Yellow River—Bohai Sea mixing zone via natural geochemical tracers, submitted to *Continental Shelf Research*, 2008] and all conservative constituents dissolved in the water.

2.3. Radium Time Series Model

[16] In addition to determining coastal transport rates, we can use radium as a tracer to quantify SGD rates. At our

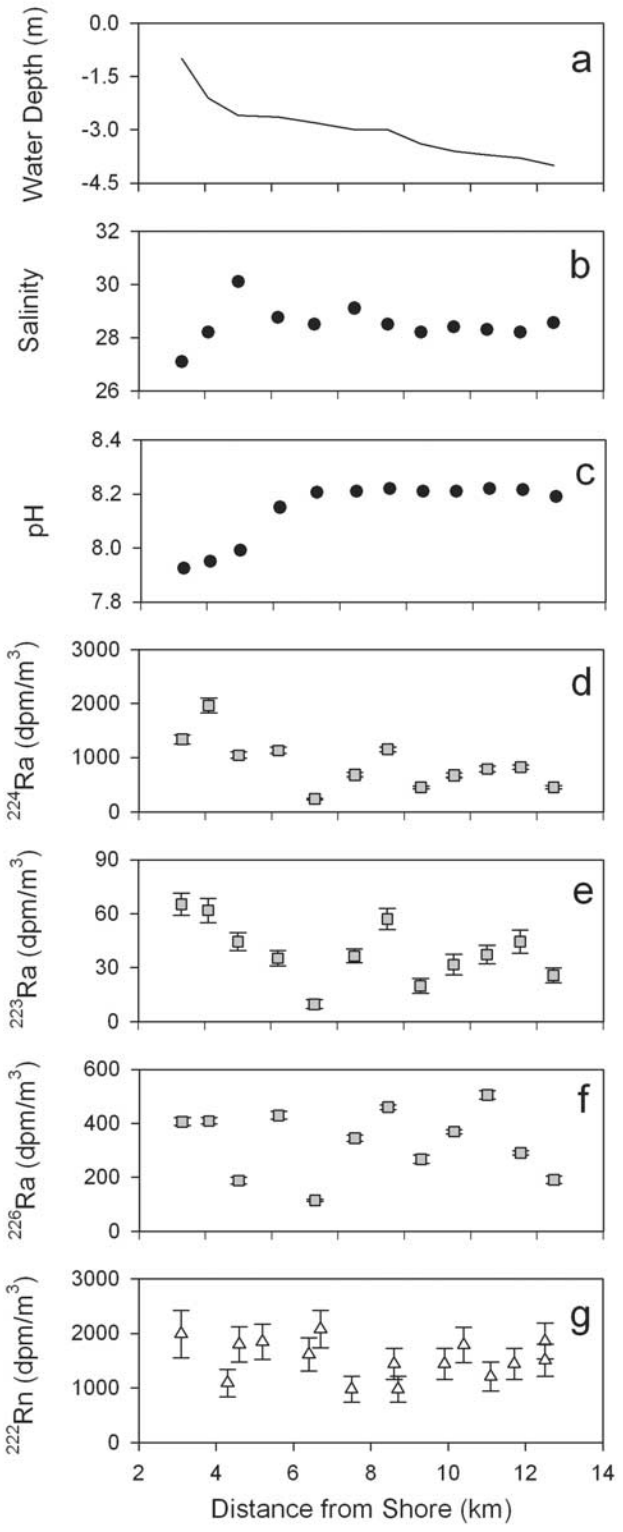

Figure 2. Profile of (a) seafloor bottom and distribution of (b) salinity, (c) pH, (d) ^{224}Ra, (e) ^{223}Ra, (f) ^{226}Ra, and (g) ^{222}Rn along offshore transect from the study site. Error bars reflect 1-σ measurement uncertainties.

study sites, the only inputs of radium should be from the Bohai Sea shelf waters (assumed to be very low), desorption from suspended sediments, desorption and subsequent diffusion from bottom sediments, and advection of groundwater into the overlying water column. The only important sink for radium on an hourly basis is mixing.

[17] We have assumed that we can neglect riverine inputs at this location because the seasonal currents in the Bohai Sea carry the Yellow River freshwater plume away from our site and because there are no other significant rivers discharging in this area. Several authors have demonstrated that during the summer months, the monsoonal winds blow from the south in this region, thus creating a cyclonic gyre within the Bohai Sea [*Hainbucher et al.*, 2004; *Wang et al.*, 2007]. Since the Yellow River is located 40 km north of our study site and its plume is directed further to the north in the summer, it is very likely that it has no influence over the tracers at our study site.

[18] Our model to quantify SGD from radium adjusts the measured radium activities (per square meter of seabed) for offshore mixing contributions and sedimentary inputs to define an excess radium inventory that must be supplied by SGD. It is difficult to accurately assess the effect of mixing on our measured inventories, because we are sampling at one point within a large, shallow continental shelf. Currents and tidal forces move water in all directions, so determining an offshore ''end-member'' value for radium activity is inappropriate. Instead, we choose to use the lowest activity measured during the course of each time series as an indicator of the shelf-wide ''background'' radium activity. As some of this radium may be supplied by SGD, this should represent a maximum estimate of non-SGD sources of radium and therefore will lead to conservative SGD estimates.

[19] Desorption from sediments is likely a significant source of radium to these shelf waters, especially for the short-lived isotopes. These waters are saline (S $\sim$ 29), so we can assume that any radium initially present upon original input of the sediments has already been desorbed. Therefore, the only source of desorbable radium on both the suspended and bottom sediments is from decay of the radium parents (insoluble thorium). By accounting for the ''background'' radium activity as described above we should have already accounted for diffusive and desorptive inputs from sediments.

[20] The following steps were used to derive SGD rates from a time series of radium samples:

[21] 1. Adjust each measured radium activity (Ra_{total}) to represent the excess radium activity by subtracting out the shelf background radium activity (Ra_{bkgd}; taken as the lowest measured concentration for each time series). This correction also accounts for the contribution from bottom and suspended sediments as described above.

[22] 2. Multiply by the measured water depth (d) to convert from excess activities to excess radium inventories per unit area of seabed. We assume that the shallow (<3 m) water column is well mixed.

[23] 3. Divide the excess radium inventory for each time step by the estimated residence time (τ) to convert to radium fluxes.

[24] 4. Finally, divide this radium flux by the groundwater end-member radium activity (Ra_{gw}) to convert to a water

Table 1. All Groundwater Samples Collected for Radium Isotopes[a]

Groundwater Sample	Date Sampled	Location	Screened Depth (m)	Salinity (psu)	pH	^{224}Ra (dpm/m^3)	^{223}Ra (dpm/m^3)	^{226}Ra (dpm/m^3)	^{222}Rn (dpm/m^3)
DO-34	18 Sep 2004	37°33.268′N, 118°43.637′E	3.0	3.0	6.34	1600 ± 120	69 ± 25	710 ± 110	-
DO-33	18 Sep 2004	37°35.357′N, 118°32.535′E	12.0	0.7	6.15	441 ± 45	16 ± 10	32 ± 82	-
N-10	18 Sep 2004	37°43.737′N, 118°45.862′E	4–10, 14–19	3.2	7.44	1620 ± 98	49 ± 18	440 ± 120	-
N-10	8 May 2005	37°43.737′N, 118°45.862′E	4–10, 14–19	12.4	7.65	3170 ± 190	39 ± 13	726 ± 54	-
N-8	8 May 2005	37°42.344′N, 118°53.224′E	1–6, 8–19	16.3	-	4100 ± 300	88 ± 20	685 ± 30	-
N-12	22 Sep 2006	37°35.698′N, 118°43.687′E	20	55.0	6.96	2950 ± 210	102 ± 16	590 ± 21	-
N-6[b]	19 Jul 2007	37°39.531′N, 118°55.753′E	2–6, 12–20	21.0	7.18	1900 ± 120	72 ± 16	189 ± 18	244,000 ± 23,000
N-7[b]	19 Jul 2007	37°40.591′N, 118°53.964′E	1.5–7, 8–12, 16–20	9.1	7.19	2100 ± 120	31 ± 11	805 ± 80	390,000 ± 60,000
N-8[b]	19 Jul 2007	37°42.344′N, 118°53.224′E	1–6, 8–19	15.8	6.96	7180 ± 410	158 ± 21	344 ± 24	351,000 ± 21,000
N-10[b]	19 Jul 2007	37°43.737′N, 118°45.862′E	4–10, 14–19	17.9	7.18	3060 ± 150	60 ± 12	950 ± 57	361,000 ± 22,000
PW-1	20 Jul 2007	37°34.054′N, 118°59.264′E	0.5	-	-	-	-	-	127,000 ± 36,000
PW-2[c]	20 Jul 2007	37°34.054′N, 118°59.264′E	0.5	27.1	7.1	15,000 ± 660	311 ± 52	780 ± 110	137,000 ± 48,000
PW-3	20 Jul 2007	37°35.605′N, 119°02.370′E	0.5	-	-	-	-	-	226,000 ± 58,000
PW-4a	22 Jul 2007	37°36.432′N, 119°00.866′E	0.5	28.3	7.15	4750 ± 270	217 ± 46	560 ± 120	193,000 ± 31,000
PW-4b	22 Jul 2007	37°36.432′N, 119°00.866′E	0.5	-	-	-	-	-	192,000 ± 29,000
PW-5	22 Jul 2007	37°36.234′N, 119°01.197′E	0.5	-	-	-	-	-	269,000 ± 30,000

[a]Samples included in upper portion of table were collected from boreholes throughout the Yellow River delta. Samples named "PW" are collected pore water samples from the study site. All radionuclide activities have been decay corrected to the time of sampling. Uncertainties shown are at the 1-σ level. psu, practical salinity units.
[b]Denotes groundwater samples used to determine AR_i and end-member values.
[c]Denotes pore water sample used to determine uncertainty range in SGD.

flux. This approach may be expressed by the following equation:

$$SGD(m/day) = \frac{\left\{\left[Ra_{total}(dpm\ m^{-3}) - Ra_{bkgd}(dpm\ m^{-3})\right] \cdot d(m)\right\}}{\tau(days) * Ra_{gw}(dpm/m^3)} \quad (2)$$

2.4. Radon Time Series Model

[25] The model used to quantify SGD using ^{222}Rn is described in detail by *Burnett and Dulaiova* [2003]. Briefly, each excess radon inventory (activity minus the radon supported by dissolved ^{226}Ra) is adjusted for atmospheric losses [*MacIntyre et al.*, 1995]. The changes in inventories between time steps are then taken to be the net radon flux over each sample interval. The maximum negative fluxes are assumed to be a conservative estimate of offshore mixing losses. These mixing losses are then added back into the radon flux, which is divided by the groundwater radon activity to achieve an SGD flux for each time step. This model has proven effective in many different environments, and therefore serves as a useful comparison [e.g., *Burnett et al.*, 2006b, 2007].

3. Results

3.1. Offshore Transport

[26] Horizontal transects of our tracers reveal some interesting patterns. Figure 2 shows the bathymetry (Figure 2a) as well as the distribution of salinity (Figure 2b), pH (Figure 2c), radium isotope activities (Figures 2d, 2e, and 2f), and ^{222}Rn activity (Figure 2g) along our offshore transect in July 2007. These plots suggest that nearshore, a source of water contributes relatively fresh water, with lower pH and generally higher radium content. According to the sampled groundwater parameters shown in Table 1, most groundwaters have lower salinity and pH than the coastal waters. Also, water table contours on land [*Chen et al.*, 2007; *Taniguchi et al.*, 2008] indicate flow in this direction. Therefore, groundwater seepage is likely in this coastal region. The short-lived radium isotopes also reveal possible groundwater inputs around 7.5 km and between 10 and 12 km offshore.

[27] Applying the model represented by equation (1) to the radium transect results in a general increase in apparent radium ages in the offshore direction (Figure 3). For this

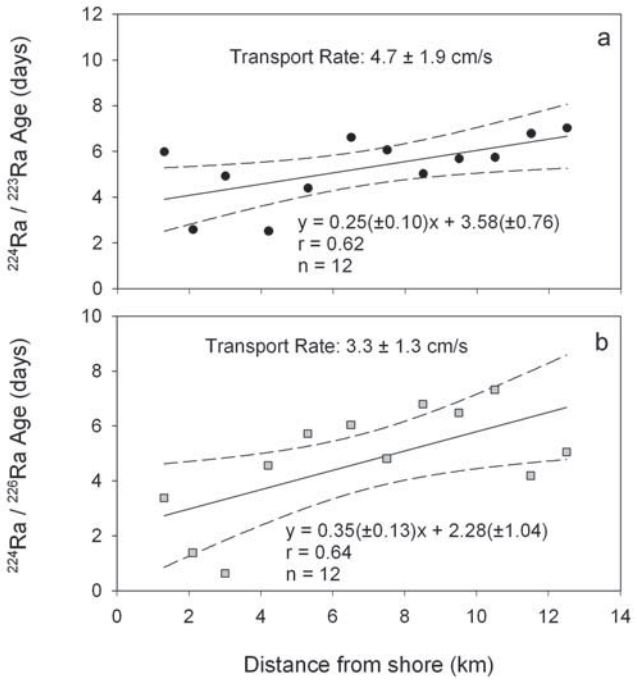

Figure 3. Distribution of apparent radium ages offshore based on the (a) ^{224}Ra/^{223}Ra AR and the (b) ^{224}Ra/^{226}Ra AR. Dashed lines represent the 95% confidence level of the linear regression. Transport rates are converted into units of cm s^{-1} from the reciprocal of the slope of the linear regression.

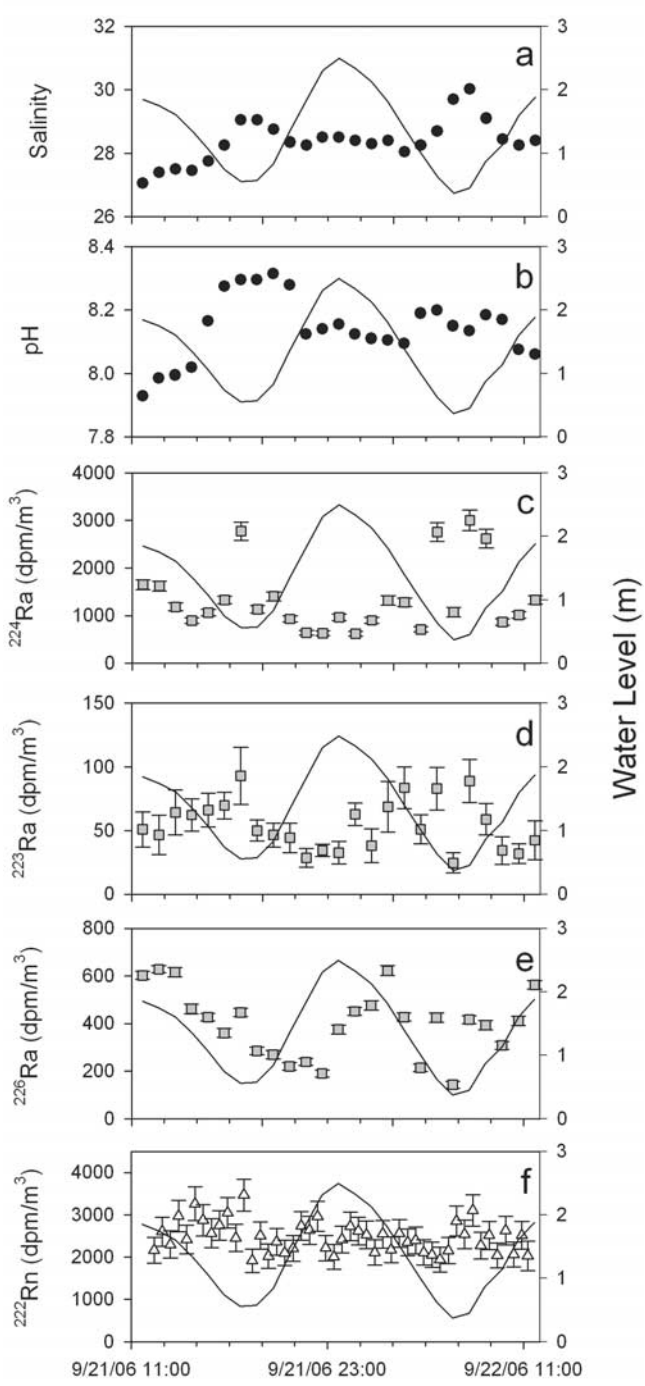

Figure 4. (right) Temporal variability of the water level as well as (a) salinity, (b) pH, (c) ^{224}Ra, (d) ^{223}Ra, (e) ^{226}Ra, and (f) ^{222}Rn during TS-1 in September 2006. Error bars represent 1-σ measurement uncertainties.

calculation, the initial AR was taken as the average AR of the saline groundwater wells sampled in 2007 (N-6 through N-10; Table 1). Even if a different initial AR was chosen, the absolute ages would change but the trend offshore would remain the same. We calculated radium ages on the basis of both the ^{224}Ra/^{223}Ra AR (a; initial AR = 44.3) and the ^{224}Ra/^{226}Ra ratio (b; initial AR = 6.23) in Figure 3. Fitting a linear regression through these data yields a time-integrated average horizontal transport rate of dissolved substances in the surface water [*Moore and Krest*, 2004]. The resulting transport rates of 4.7 and 3.3 cm s^{-1} based on the inverse of the slope of the respective regression lines are not significantly different. Peterson et al. (submitted manuscript, 2008) determined that the coastal mixing rates off the mouth of the Yellow River (1.4–1.6 cm s^{-1}) did not vary significantly with river discharge within the range of discharges studied (81–568 m^3 s^{-1}), and concluded that mixing was tidally driven. Because there are no other significant advective mixing forces in this study area, we find that tidal forces must have an even greater effect at transporting dissolved substances offshore in the shallow tidal flats where this study was conducted.

3.2. Radium Time Series

[28] Radium samples were collected hourly for 25 hours in September 2006 (TS-1) at a fixed location 1 km from shore, and for 23 hours in July 2007 (TS-2) at another station along the same line but located 2 km from shore. These sample sets are useful in that they are not simply a snapshot image of tracer concentrations at this site, but allow us to examine how the tracers behave over a complete tidal cycle. One might expect, for example, to find the highest SGD rates during low tide, as has been found in several other settings [e.g., *Burnett et al.*, 2007; *Swarzenski et al.*, 2007b]. The low tides here during TS-1 correspond with increases in salinity and pH (Figures 4a and 4b), so the composition of the enhanced SGD during low tide, as indicated by the peaks in radium (Figures 4c, 4d, and 4e), appears to be influenced by recirculated seawater and saline groundwater. The peak salinity and pH values during the low tides are very similar to those sampled offshore (>5 km, Figure 2).

[29] The radium trends indicate input during the low/ebb tides. Sharp peaks occur in the short-lived radium isotope record at the low tides, while the ^{226}Ra tends to peak on the falling tide. The model is based on calculating radium fluxes, so the greatest change in inventories actually occurs during the downgoing tide. Because the tidal range in this area is nearly 2 m, this shallow environment is greatly influenced by tidal forces.

[30] The tracer record from TS-2 (Figure 5) shows little temporal variability in the salinity record, but indicates decreases in pH corresponding with the low tides. These behaviors suggest a more significant fraction of terrestrial water in the discharging groundwater than that observed during the 2006 time series when the salinity and pH increased at low tide. This terrestrial component is not necessarily fresher than the overlying water. Several groundwaters sampled (Table 1) show saline to hypersaline conditions while still maintaining relatively low pH.

[31] The short-lived radium trends seen in these data are similar to those from TS-1. All three radium isotopes show sharp increases at or shortly before low tide, i.e., generally on the falling tides. Although ^{226}Ra tended to precede the short-lived radium peaks in TS-1, it behaved much more like ^{223}Ra and ^{224}Ra during TS-2 by maintaining a baseline activity throughout the high tides. One interesting observation from these data, however, is that the radium peaks occur during the falling tide, whereas the peaks in pH appear a few hours earlier in TS-2.

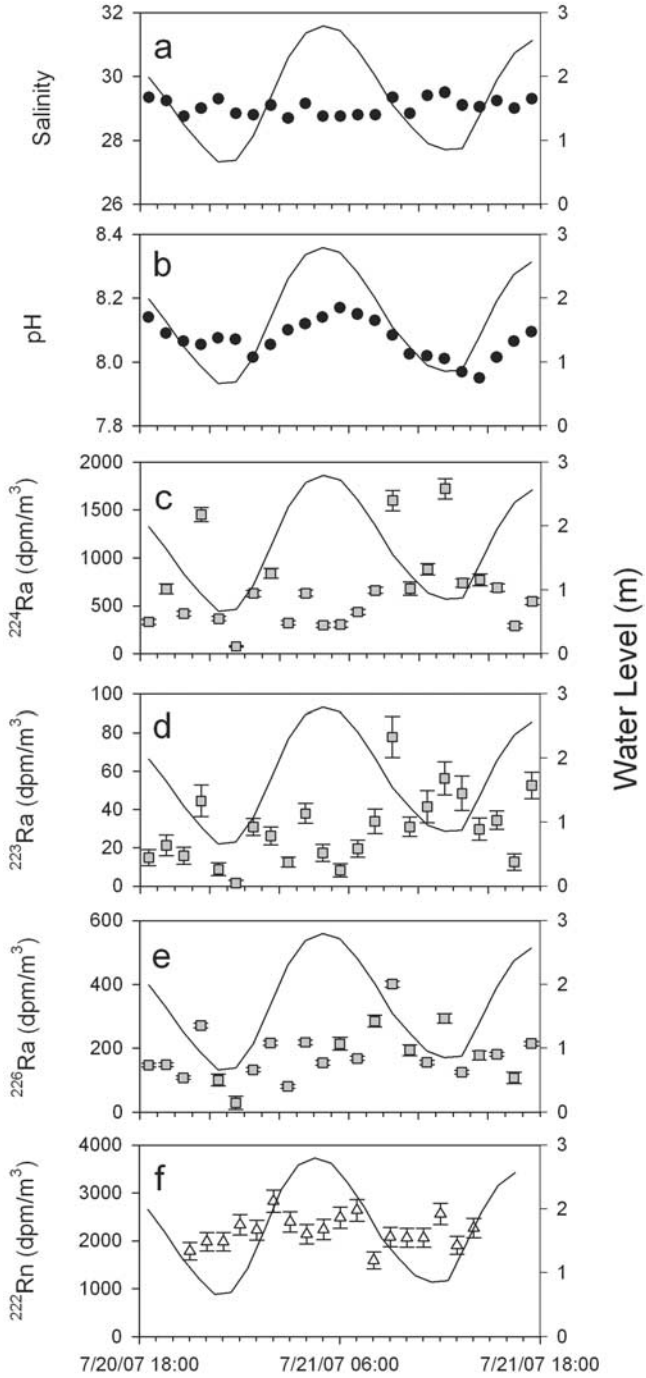

Figure 5. Temporal variability of the water level (right axis) as well as (a) salinity, (b) pH, (c) ^{224}Ra, (d) ^{223}Ra, (e) ^{226}Ra, and (f) ^{222}Rn during TS-2 in July 2007. Error bars represent 1-σ measurement uncertainties.

[32] We used the radium isotopic data with the model described in section 2.3 (equation 2) to quantify the groundwater discharge rates. The calculations are based on a unit area of sea bottom, and give results in terms of specific fluxes (m^3 m^{-2} d^{-1}) or vertical velocities of the advecting water (m d^{-1}). Table 2 summarizes important parameters used in the calculations. The following section details each of the calculations steps, as well as the choice of the parameters reported in Table 2.

3.2.1. Adjust Measured Radium Activities for Background Radium

[33] The time series radium trends indicate that each isotope achieves a baseline or ''background'' activity throughout the tidal cycle, but always remains present above detection. We elect to use the lowest activity measured for each radium isotope during the course of each time series sampling to represent this ''background.'' In other words, we interpret these activities as those that would be present with no SGD signal, i.e., 100% of the radium is derived from other sources such as desorption from particles and shelf waters mixing into the sampling area. Using the lowest measured activity thus represents a conservative estimate of the background activity, because these samples could still contain some groundwater-derived radium. The selected shelf background activities for TS-2 are uniformly lower than TS-1 (Table 2). This difference is likely a reflection of its location being further offshore. These background values are subtracted from all other measurements within the time series to correct each sample for the shelf contribution to yield an excess radium activity.

[34] Diffusive inputs from bottom sediments and desorption of radium from suspended sediments are already considered when subtracting out the background activity as described above. These input rates are assumed to be uniform over time and space. There is no direct source of suspended sediments to our study site, so we assume that the suspended sediments in this area are derived from resuspended bottom sediments and no further sedimentary radium input corrections are necessary.

3.2.2. Convert From Excess Radium Activity to Excess Radium Inventory

[35] In order to remove the effect of different water depths associated with these samples, we multiply each excess radium activity concentration by the water depth at the time of sampling to convert to an excess radium inventory. This correction allows for a direct comparison of the absolute radium activities per unit area of seabed.

3.2.3. Divide the Excess Radium Inventories by the Water Residence Time

[36] In order to convert excess inventories to a flux rate, we must divide by the effective residence time of the coastal

Table 2. Radium Time Series Model Parameter Summary[a]

	TS-1 (dpm m^{-3})	Common (dpm m^{-3})	TS-2 (dpm m^{-3})
	Shelf Background Activity		
^{224}Ra	625		77.8
^{223}Ra	24.7		1.5
^{226}Ra	143		28.8
	Groundwater End-Member Radium Activity		
^{224}Ra		3560	
^{223}Ra		80	
^{226}Ra		570	
	Pore Water End-Member Radium Activity		
^{224}Ra		15,000	
^{223}Ra		311	
^{226}Ra		780	

[a]The values found in the central column between TS-1 and TS-2 are common to both time series.

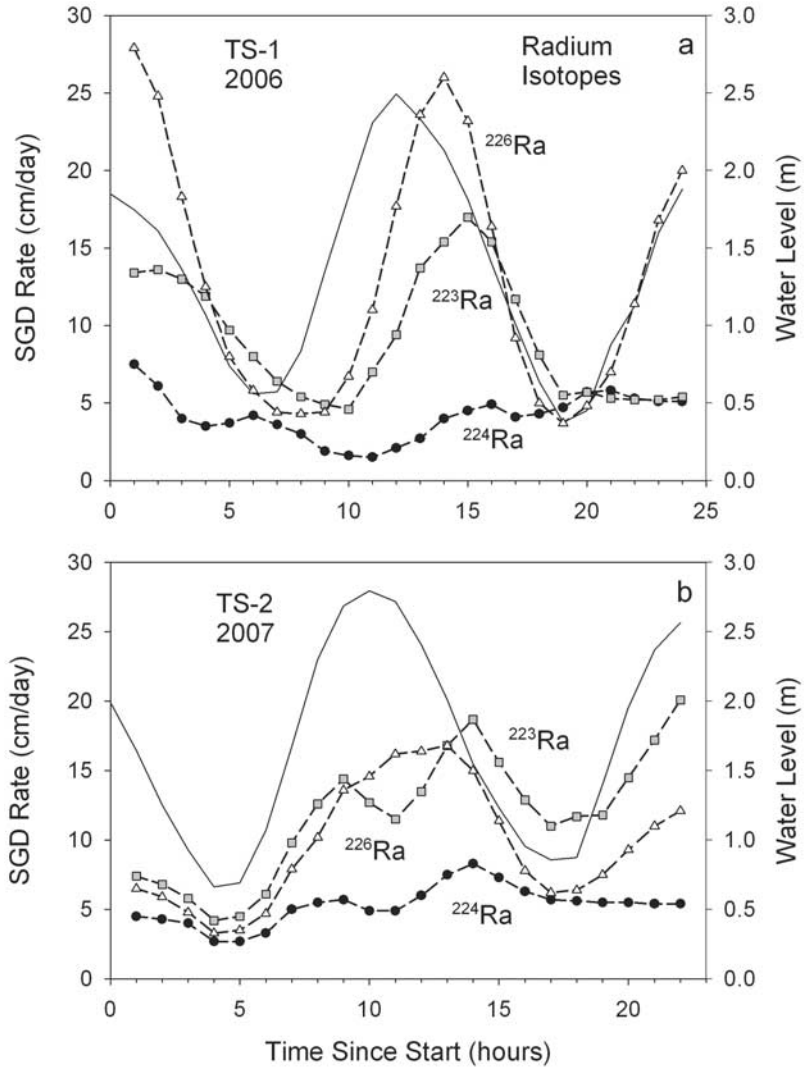

Figure 6. Radium time series results for SGD fluxes during (a) TS-1 and (b) TS-2 as well as the corresponding water level recorded at the study site. Results from ^{224}Ra are shown by the black circles, those from ^{223}Ra are shown by gray squares, and those from ^{226}Ra analysis are shown by white triangles. The results shown represent a three-point smoothing.

waters. We elect to use an average apparent radium age of the waters sampled along the offshore transect based on the ^{224}Ra/^{226}Ra AR (Figure 3). The measurement uncertainty associated with ^{226}Ra (~10%) is much better than that of ^{223}Ra (~25%), so this provides the best residence time estimate available (4.7 days).

[37] While we think this is a reasonable estimate on the basis of the data available, there are some uncertainties. The model used to calculate the apparent radium ages from water samples (equation 1) assumes only one source of radium with a fixed isotopic composition. However, the offshore radium trends reveal possible groundwater inputs around 7.5 km and between 10 and 12 km offshore (Figure 2). If these are indeed related to groundwater inputs, our assumption would still hold as long as the radium signature is the same. Unfortunately, we do not have any means to assess such variations at this time. In view of these difficulties, we later address the model effects of different effective residence times in a section on uncertainties (4.3).

3.2.4. Divide by the End-Member Value to Convert Into a Water Flux

[38] Table 1 presents a wide range in possible groundwater end-members found throughout the delta that could constitute the advecting groundwater fluids. Only small volumes (~10 L) of sediment pore water could be collected for radium analysis, so we feel that the large range found in pore water radium results are at least partially due to analytical difficulties associated with insufficient sample volumes. We have elected to use the average of the saline wells measured in July 2007 (N-6 through N-10). These wells are all directly up-gradient of the study site and were collected immediately after one of our time series (TS-2), so likely represent the terrestrial source water component of the SGD. No detectable freshening of the surface waters during the apparent discharge intervals of the time series occurred, so the use of fresh groundwater end-members (e.g., wells sampled in 2004, Table 1) is not appropriate. The initial groundwater ARs used to find the radium ages

Table 3. Summary of the Results of the SGD Analyses Based on Radium Isotopes, Radon, and Automatic Seepage Meters Deployed in the Same Area[a]

	TS-1 (cm d^{-1})		TS-2 (cm d^{-1})	
	SGD Rate	s.d.	SGD Rate	s.d.
^{224}Ra	4.5 (1.1)	3.4 (0.8)	5.2 (1.2)	3.0 (0.7)
^{223}Ra	9.4 (2.4)	6.2 (1.6)	11.8 (3.1)	8.5 (2.2)
^{226}Ra	13.9 (10.2)	11.1 (8.1)	9.6 (7.1)	6.2 (4.5)
^{226}Ra offshore distribution	-	-	24.2	-
^{222}Rn	13.8	17.9	8.4	11.8
Seepage meters (2006 results)				
1000/1500 m from shore	42.2	27.9	35.6	19.9
2000 m from shore	48	44	n/A	n/A
3000 m from shore	130	117	n/A	n/A
4000 m from shore	n/A	n/A	67.2	43.9
5000 m from shore	16	14	15.9	12.6
6000 m from shore	33	33	n/A	n/A
7000 m from shore	15	14	n/A	n/A

[a]The rates reflect the average SGD rate (cm d^{-1}) throughout the time series, with the corresponding standard deviation for each set. Values in parentheses are based on an end-member equivalent to the highest pore water radium measured. Seepage meter results from *Taniguchi et al.* [2008]. n/A, not applicable.

from the offshore transect are also based on the average of these selected groundwater samples.

[39] Dividing the radium fluxes by the groundwater end-member activities yields estimates of the SGD flux required to support the measured excess inventories. Figures 6a and 6b show the model results for TS-1 and TS-2, respectively. The three isotopes show similar patterns, though their range in SGD rates varies significantly. All isotopes indicate high discharge during the falling tide for both TS-1 and TS-2. Table 3 summarizes the results from each time series model. During TS-1, SGD rates averaged 4.5, 9.4, and 13.9 cm d^{-1} based on ^{224}Ra, ^{223}Ra, and ^{226}Ra, respectively. TS-2 SGD rates were similar, averaging 5.2, 11.8, and 9.6 cm d^{-1} based on the same isotopes.

3.3. Radon Time Series

[40] Figures 4f and 5f show the results of the ^{222}Rn time series analysis from TS-1 and TS-2, respectively. Measurements were integrated over 30 min for TS-1, and over 1 hour for TS-2 in order to achieve better analytical uncertainties. In both cases, no clear temporal trends in the radon activities were observed over the tidal cycle, except a slight increase in radon activity during the low tides of TS-1. The water depth changes throughout this tidal cycle, however, so significant changes in the radon inventories do exist. The model presented by *Burnett and Dulaiova* [2003] requires knowledge of the offshore radon activity to account for radon introduced during the flood tide. We use the minimum value sampled along the offshore transect (980 disintegrations per minute (dpm) m^{-3} at 7.5 and 8.7 km offshore) as the offshore radon end-member. Values in the range of ~1000 dpm m^{-3} are found at several locations along the transect, so we feel this is a reasonable choice.

[41] We also must apply a groundwater end-member to this model. Because the radon in groundwater analysis requires much less water than that for radium (250 mL versus 10+ L), we were able to collect water samples for radon from additional pore water locations than those sampled for radium (Table 1). The average (and standard deviation) radon activity from 5 pore waters sampled was 191,000 ± 54,000 dpm m^{-3}, so we take this to represent the groundwater end-member. This value is somewhat lower than the average from the monitoring wells on land (average = 337,000 ± 64,000 dpm m^{-3}). Sampling the pore waters in this case is a more direct assessment of the composition of the actual advecting SGD water, so should provide a better constrained end-member value than the terrestrial boreholes selected for the radium end-members.

[42] Wind speeds (and thus radon loss via atmospheric evasion) observed during TS-1 (average = 3.4 m s^{-1}) were somewhat higher than those during TS-2 (average = 2.9 m s^{-1}), so we applied a shorter integrated mixing time for TS-1 (1 hour versus 3 hours for TS-2) as required by the model. This mixing time determines the number of hours that the maximum negative fluxes are extrapolated to represent mixing losses. A shorter mixing time minimizes the risk of overestimating mixing losses for other samples on the basis of a large negative flux from one sample.

[43] Figures 7a and 7b show the model results of the SGD rates based on ^{222}Rn from TS-1 and TS-2, respectively. The results from both TS-1 and TS-2 show enhanced SGD during the falling tides as did the radium isotope analyses. The average SGD rates for the two time series are 13.8 cm d^{-1} (TS-1), and 8.4 cm d^{-1} (TS-2), which are within the range of the radium results presented in section 3.2.4.

3.4. Offshore Radium Distribution Assessment of SGD

[44] From the offshore transect data presented in Figure 2, we can use the distribution of ^{226}Ra to independently calculate shelf-wide SGD rates as per the paper by *Moore* [1996]. He found enrichments of ^{226}Ra in shelf waters along the southeastern United States and applied a version of the following equation to determine regional SGD rates:

$$SGD(m/day) = \frac{Excess^{226}Ra(dpm\ m^{-1}) \cdot d(m)}{\tau(days) \cdot {}^{226}Ra_{gw}(dpm\ m^{-1})} \quad (3)$$

[45] In this equation, the excess ^{226}Ra represents the average activity of ^{226}Ra that is enriched above the open ocean background level. Using the lowest activity measured along the transect (115 dpm m^{-3}) as the oceanic background level, we find the average excess activity along the transect to be 322 dpm m^{-3}. The excess ^{226}Ra activity used is therefore 207 dpm m^{-3}. The average depth (d) along the transect was 3.0 m. We take the average ^{224}Ra/^{226}Ra age of the samples (4.7 days; Figure 3) as the residence time of the shelf waters (τ) and the groundwater end-member value of 570 dpm m^{-3} (Table 2) as the $^{226}Ra_{gw}$ term. After applying equation (3) to our results, we find the regional vertical velocity of SGD to be 24.2 cm d^{-1}. This SGD flux (Table 3) is similar but somewhat higher than those determined by the radium model in section 3.2.

4. Discussion

4.1. Radium Offshore Distribution

[46] The short-lived radium isotope distribution in Figure 2 shows several peaks farther offshore, indicating either possible groundwater inputs around 7.5 km and 11 km offshore or pulses of tidal currents that have carried coastal

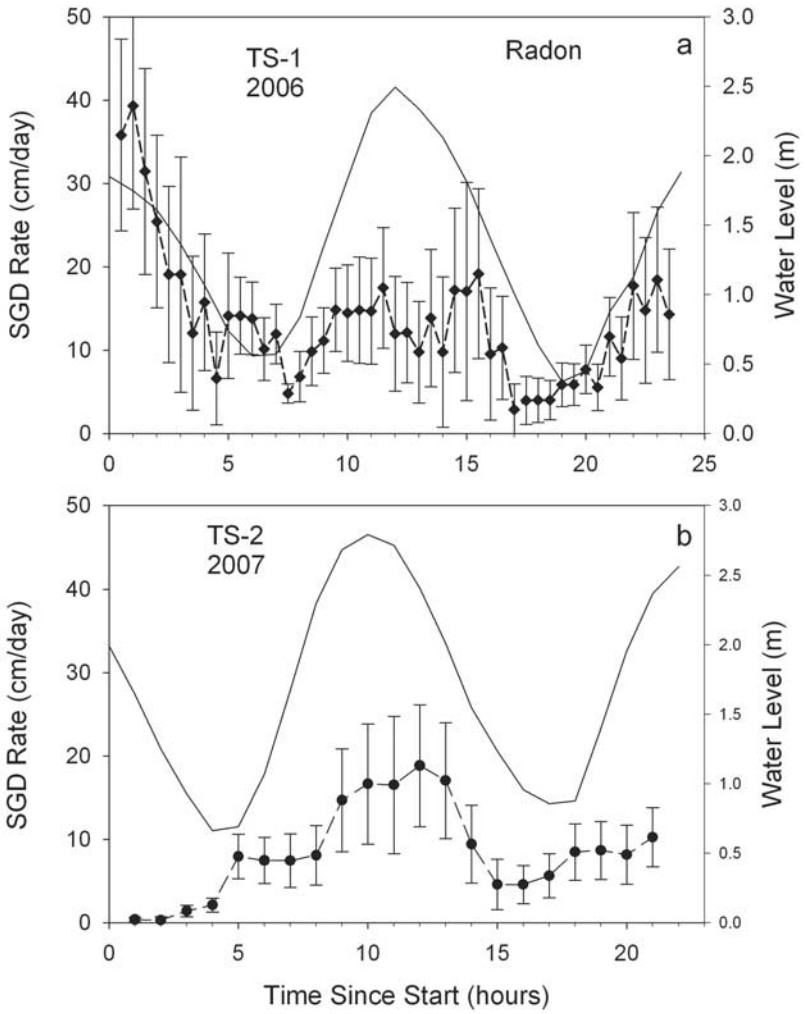

Figure 7. Results from the ^{222}Rn SGD model for (a) TS-1 and (b) TS-2 as well as the corresponding water level recorded at the study site. The results shown represent a five-point smoothing. Error bars shown are propagated errors throughout the model calculations.

waters offshore. The relative amplitudes of these peaks becomes more pronounced for the longer-lived isotopes (i.e., ^{224}Ra < ^{223}Ra < ^{226}Ra), as is expected for aging water masses, but we lack sufficient data to determine whether these peaks are due to local groundwater inputs or are the result of coastal waters mixing offshore. Further investigations at this and other study sites should look into this possibility further, as done by *Hancock et al.* [2006].

4.2. Radon Results

[47] A possible source of error in the radon model used to find SGD rates is that significant inputs of radon could be from diffusion into the water column from the sediments. We have estimated this input by using an empirical equation reported by *Burnett et al.* [2003b] to relate the ^{226}Ra content in sediments ($^{226}Ra_{sed}$; units = dpm g^{-1}) to the diffusive flux of ^{222}Rn:

$$^{222}RnFlux\left(dpmm^{-2}d^{-1}\right) = 495 \cdot {}^{226}Ra_{sed} + 18.2 \qquad (4)$$

[48] We have measured several sediment samples via gamma spectrometry, and found the average ^{226}Ra activity to be 1.62 dpm g^{-1} (Table 4). Applying equation (4), the corresponding ^{222}Rn flux is thus 820 dpm m^{-2} d^{-1}, or 34.2 dpm m^{-2} h^{-1}. Assuming this system is in steady state, we can find the ^{222}Rn concentration supported by diffusion in the water column by subtracting each calculated hourly atmospheric flux from the diffusive flux, then dividing by the decay constant (0.0076 h^{-1}) and by the average water depth for each measurement interval [*Dulaiova et al.*, 2006]. This calculation results in nearly every measurement interval showing a negative value for the supported ^{222}Rn activity. Therefore, we conclude that on average, the atmospheric evasion losses are greater than the diffusive flux of radon from the bottom sediments, and as such, we can neglect this possible source of ^{222}Rn.

[49] *Mulligan and Charette* [2006] have pointed out that using ^{222}Rn as a tracer to model SGD yields total discharge rates, because radon would be present in both the terrestrial component as well as the recirculated seawater component of the discharging groundwater. Using radium as the tracer, however, would only reveal the recirculated seawater (saline) flow, as radium remains particle bound in

Table 4. Summary of ^{226}Ra Content on Collected Sediments, Measured via Gamma Spectrometry[a]

Sediment Sample Name	Collection Date	Latitude	Longitude	Salinity (psu)	^{226}Ra Activity (dpm g^{-1})
Yellow River Suspended	15 Sep 2004	37°45.666′N	119°09.327′E	0	2.23 ± 0.16
Yellow River Bottom I	4 May 2005	37°45.666′N	119°09.327′E	0	1.36 ± 0.08
Yellow River Bottom II	4 May 2005	37°45.666′N	119°09.327′E	0	1.39 ± 0.19
Yellow River Bottom III	19 Sep 2006	37°45.666′N	119°09.327′E	0	1.49 ± 0.11
TS-1	22 Sep 2006	37°36.525′N	119°00.518′E	28.6	1.97 ± 0.12
Yellow River Bottom IV	19 Jul 2007	37°45.666′N	119°09.327′E	0	1.26 ± 0.15
Average					1.62 ± 0.14

[a]All samples except TS-1 were collected in the Yellow River, above the maximum salinity front. Uncertainties shown represent 1-σ measurement uncertainties.

freshwater. This theory agrees with our results and because the radium fluxes are as high or higher than those determined from radon, the vast majority of SGD at our study sites is composed of recirculated seawater. The exception to this is the ^{224}Ra results during TS-1, when the radium result was roughly one third of that determined by the radon.

4.3. Model Uncertainties

[50] The radium model results in section 3.2 show similar patterns among the different isotopes, but the absolute fluxes determined by ^{224}Ra are consistently lower than those found by ^{223}Ra and ^{226}Ra. This difference is likely a result of overestimating the shelf background ^{224}Ra activity by using the lowest sampled activity during the time series. If these lowest samples still contained a ^{224}Ra component from SGD, then we overcompensated and caused the ultimate SGD fluxes to be too low.

[51] This discrepancy may also be a result of our limited selection of groundwater end-member values. While we are most confident that the saline groundwaters sampled in July 2007 represent the most likely end-member values, the sampled pore waters were consistently higher in measured radium activity. In order to assess the model uncertainty due to end-member selection, we applied the model using the highest pore water sample (PW-2; see Tables 2 and 3). The model results based on this end-member are shown in Table 3. Using this extremely high pore water value as the end-member, the average SGD fluxes decrease by 75% for ^{224}Ra and ^{223}Ra, and by 25% for ^{226}Ra. Another source of uncertainty in the model involves diffusive inputs of radium to the water column as intertidal sediments are flooded during each high tide. We do not feel that this process represents an important source of radium as the tidal variations in ^{226}Ra (too long-lived to regenerate on tidal timescales) are about the same as the observed ^{224}Ra variations.

[52] One other source of uncertainty in the radium model concerns the residence time of these coastal waters. We used a value of 4.7 days, based on the average ^{224}Ra/^{226}Ra age from Figure 3, but as detailed in section 3.2.3, several sources of uncertainty exist in this calculation. If a longer water residence time were used, for example the average ^{224}Ra/^{223}Ra age from Figure 3 (5.3 days; an increase of 13%), the modeled SGD rates would decrease by 11%. Using a shorter residence time (4.1 days; a decrease of 13%), the corresponding modeled SGD rates would increase by 15%.

[53] *Burnett et al.* [2007] summarize the important uncertainties behind the radon model used here. As with the radium model, the most significant source of uncertainty lies with assigning an end-member value to the discharging fluids. In addition, assessing the mixing losses of radon to both the offshore waters and the atmosphere represent other, yet often less important, sources of uncertainty.

4.4. Comparison to Seepage Meters

[54] Table 3 indicates that our different geochemical tracer analysis techniques for quantifying SGD rates are in reasonable agreement. We also have some estimates based on a completely independent approach. Figures 8a and 8b contain data presented by *Taniguchi et al.* [2008] for automatic seepage meter fluxes collected nearby and at the same time as our TS-1 and TS-2 time series experiments, respectively. The seepage meter location during TS-2 was 500 m inland of the tracer sampling location, whereas that corresponding with TS-1 was ~50 m from our sampling station. Also, a Darcy's Law hydrological calculation of the terrestrial groundwater flow to the ocean in this area using FEFLOW shows results ranging from 0.3 to 5.8 cm d^{-1} (J. Z. Cheng, personal communication, 2008).

[55] Our interpretive SGD trends based on the radium results agree very well with the seepage meter patterns for both periods. The patterns based on the radon records also resemble those of the seepage meters, but with less smooth trends. A disadvantage of seepage meters is that they can only integrate over the small area of sea bottom they cover (~0.25 m^2), but the chemical tracers integrate over an unknown yet much greater spatial range [*Burnett et al.*, 2006b]. Nonetheless, the general agreement in patterns of SGD between the tracer methods and the seepage meters provides confidence in both approaches.

[56] During the period of chemical tracer sampling of TS-1, the seepage meter average SGD rate was high at 42.2 ± 27.9 cm d^{-1} (Table 3), of which ~3% was fresh groundwater discharge according to salinity measurements made inside the seepage meter chambers. Averaging the seepage meter fluxes over several days prior to the tracer sampling provides an average SGD flux of 20.7 ± 20.5 cm d^{-1}, closer to our tracer-derived values. Seepage meter averages from other nearby locations during TS-1 ranged from 15 to 130 cm d^{-1} [*Taniguchi et al.*, 2008].

[57] The average seepage meter flux during our sampling of TS-2 was also high at 35.6 ± 19.9 cm d^{-1}, of which about 21% was fresh groundwater. The several day integrated average SGD based on this seepage meter was similar at 41.9 ± 20.4 cm d^{-1}. The fraction of fresh groundwater in the SGD measured from the seepage meters indicates a

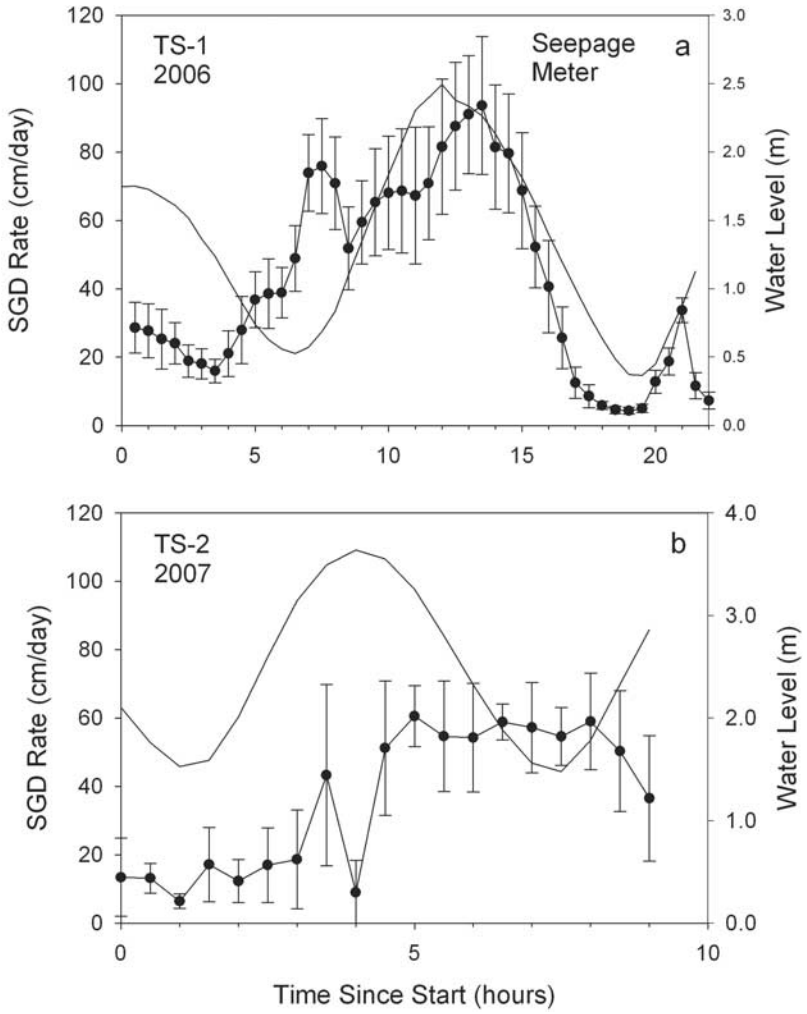

Figure 8. Independent analysis of SGD by means of automated seepage meters, as summarized by *Taniguchi et al.* [2008] for the time during (a) TS-1 and (b) TS-2 chemical tracer sampling. Error bars represent standard deviation of all measurements recorded during each measurement interval (30 min).

more pronounced recirculated seawater signal during TS-1 than during TS-2. This was also supported by our time series pH and salinity measurements.

[58] The seepage meter flux results are generally higher than the results found from our independent radium isotope and radon analyses. One possible reason for this difference is that the SGD is dominated by recirculated seawater, with a short residence time in the subsurface. From data presented by *Taniguchi et al.* [2008] on the basis of all their seepage meter results in the area, the freshwater component of SGD is never greater than 27%, and all but one sample ranged between 0.5 and 7.5%. If most of this water is simply recirculating through the sediments over a tidal cycle, it would not have sufficient time to fully equilibrate with the tracer concentrations in the aquifer. Therefore, the groundwater end-members that were used in the models above could be too high compared to their actual values, artificially lowering our modeled SGD rates. In addition, the ^{222}Rn pore water value is better constrained, lower than the borehole samples collected on land, yet produced SGD rates that were in the same range as the radium-based values.

4.5. Regional-Scale Fluxes

[59] *Taniguchi et al.* [2008] defined the offshore seepage face as being equal to a width of about 7 km, and used the length of the Yellow River delta coastline (350 km) to scale up their seepage results for comparison to the Yellow River discharge. Using these same values, and conservatively assuming that our lowest estimates of SGD (4.5 cm d^{-1} from the ^{224}Ra model during TS-1; 5.2 cm d^{-1} from the ^{224}Ra model during TS-2) are uniform over this area, we find a total flow of approximately 1280 m^3 s^{-1} during TS-1 and 1480 m^3 s^{-1} during TS-2 around the Yellow River delta, most of which is likely recirculated seawater [*Taniguchi et al.*, 2008]. For comparison, the Yellow River discharge during this time of year is around 600 m^3 s^{-1}. As these SGD fluxes are conservative values, the actual water exchange from SGD compared to the Yellow River could be much higher.

[60] As part of this study, nitrate was measured in the groundwater wells and the Yellow River to assess relative fluxes to the Bohai Sea. The average NO_3^- concentration in the groundwater wells that we sampled for radium (N-6 through N-10) was 440 μM and that in the Yellow River

was 430 μM (T. Z. Mi, personal communication, 2005). Multiplying these concentrations by the SGD fluxes yields nitrate fluxes 2 to 3 times higher than that delivered by the Yellow River. Care must be taken in interpreting these results, however, because geochemical reactions often alter the nutrient character of groundwater within the subterranean estuary [*Santos et al.*, 2008; *Spiteri et al.*, 2008].

[61] Nonetheless, *Chen et al.* [2007] have found groundwaters throughout the delta that are up to 1 order of magnitude enriched in nitrate concentration relative to that of the Yellow River, so clear potential exists for SGD to supply excess nitrate to the Bohai Sea. Previous studies have found SGD to be an important nutrient source, even in river-dominated regions, such as the Gulf of Thailand [*Dulaiova et al.*, 2006]. Application of the offshore transport rates to the flux of nutrients from a coastal source (e.g., SGD) can help assess whether the rates are sufficient to transport the nutrients offshore before uptake by primary productivity (Peterson et al., submitted manuscript, 2008). Increasing levels of dissolved inorganic nitrogen have been documented as occurring in the central Bohai Sea over the past few decades [*Zhang et al.*, 2004], so these results can help assess the source of the excess nitrogen.

5. Conclusions

[62] We have measured several groundwater tracers in an area ~40 km south of the Yellow River estuary to quantify SGD rates from offshore transects and time series analyses. Salinity and pH are useful tracers in this environment, showing increasing values in the offshore direction. The gradient in apparent radium ages of the water masses with distance from shore yields horizontal transport rates between 3.3 and 4.7 cm s^{-1}.

[63] We show that using radium isotopes to assess SGD rates via a stationary time series fashion is a valuable approach. The results from the radium time series were similar to those using an established ^{222}Rn model, and followed the patterns of SGD from seepage meter measurements. During September 2006, the average SGD rates ranged from 4.5 to 13.9 cm d^{-1}, and the discharging water was composed primarily of recirculated seawater. The SGD rates found during July 2007 averaged between 5.2 and 11.8 cm d^{-1}, and apparently have a larger fraction of terrestrial water. These fluxes and patterns are somewhat lower than those from individual seepage meters deployed nearby but are similar to average rates reported from seepage meters positioned in the same general area.

[64] There are some uncertainties associated with the radium time series model that we use to estimate the SGD fluxes. The most prominent of these uncertainties lies in the assignment of the appropriate groundwater end-member. If we use measured pore water radium activities as the end-member instead of the saline groundwaters, our SGD fluxes decrease by 75% for ^{224}Ra and ^{223}Ra, and by 25% for ^{226}Ra. Other, more minor sources of uncertainty for the model involve the residence time of the coastal waters and diffusive inputs from tidal inundation of intertidal sediments.

[65] Scaling our SGD fluxes determined from the radium isotopes to the whole Yellow River delta, we find estimated SGD and nitrate fluxes 2–3 times that of the Yellow River. We suspect that most of the regional SGD is composed of recirculated seawater. In fact, excessively high nitrate levels in groundwaters have been measured around the delta, so NO_3^- fluxes to the Bohai Sea from SGD are likely higher than those from the Yellow River, at least during periods of low river discharge.

[66] **Acknowledgments.** The authors thank Natasha Dimova for lab assistance with this project. Many thanks are owed to Jianzhong Cheng, Songqing Zeng, and all the Chinese team for logistical field support. We also thank two anonymous reviewers for their insightful comments. This work was funded and coordinated by the Project on Yellow River Studies led by Yoshihiro Fukushima through the Research Institute for Humanity and Nature. Additional support was provided by a National Science Foundation grant (OCE0350514) to W.C.B.

References

Beck, A. J., J. P. Rapaglia, J. K. Cochran, and H. J. Bokuniewicz (2007), Radium mass-balance in Jamaica Bay, NY: Evidence for a substantial flux of submarine groundwater, *Mar. Chem.*, *106*(3–4), 419–441, doi:10.1016/j.marchem.2007.03.008.

Beck, A. J., J. P. Rapaglia, J. K. Cochran, H. J. Bokuniewicz, and S. Yang (2008), Submarine groundwater discharge to Great South Bay, NY, estimated using Ra isotopes, *Mar. Chem.*, *109*(3–4), 279–291, doi:10.1016/j.marchem.2007.07.011.

Burnett, W. C., and H. Dulaiova (2003), Estimating the dynamics of groundwater input into the coastal zone via continuous radon-222 measurements, *J. Environ. Radioact.*, *69*(1–2), 21–35, doi:10.1016/S0265-931X(03)00084-5.

Burnett, W. C., G. Kim, and D. Lane-Smith (2001), A continuous monitor for assessment of ^{222}Rn in the coastal ocean, *J. Radioanal. Nucl. Chem.*, *249*(1), 167–172, doi:10.1023/A:1013217821419.

Burnett, W. C., H. Bokuniewicz, M. Huettel, W. S. Moore, and M. Taniguchi (2003a), Groundwater and porewater inputs to the coastal zone, *Biogeochemistry*, *66*(1/2), 3–33, doi:10.1023/B:BIOG.0000006066.21240.53.

Burnett, W. C., J. E. Cable, and D. R. Corbett (2003b), Radon tracing of submarine groundwater discharge in coastal environments, in *Land and Marine Hydrology*, edited by M. Taniguchi, K. Wang, and T. Gamo, pp. 25–42, Elsevier, New York.

Burnett, W. C., H. Dulaiova, C. Stringer, and R. Peterson (2006a), Submarine groundwater discharge: Its measurement and influence on the coastal zone, *J. Coastal Res.*, *39*, 35–38.

Burnett, W. C., et al. (2006b), Quantifying submarine groundwater discharge in the coastal zone via multiple methods, *Sci. Total Environ.*, *367*(2–3), 498–543, doi:10.1016/j.scitotenv.2006.05.009.

Burnett, W. C., I. R. Santos, Y. Weinstein, P. W. Swarzenski, and B. Herut (2007), Remaining uncertainties in the use of Rn-222 as a quantitative tracer of submarine groundwater discharge, in *A New Focus on Groundwater-Seawater Interactions*, edited by W. Sanford et al., *IAHS Publ.*, *312*, 109–118.

Burnett, W. C., R. Peterson, W. S. Moore, and J. de Oliveira (2008), Radon and radium isotopes as tracers of submarine groundwater discharge — Results from the Ubatuba, Brazil SGD assessment intercomparison, *Estuarine Coastal Shelf Sci.*, *76*(3), 501–511, doi:10.1016/j.ecss.2007.07.027.

Charette, M. A. (2007), Hydrologic forcing of submarine groundwater discharge: Insight from a seasonal study of radium isotopes in a groundwater-dominated salt marsh estuary, *Limnol. Oceanogr. Methods*, *52*(1), 230–239.

Charette, M. A., and M. C. Allen (2006), Precision groundwater sampling in coastal aquifers using a direct push shielded-screen wellpoint system, *Ground Water Monit. Rem.*, *26*(2), 87–93, doi:10.1111/j.1745-6592.2006.00076.x.

Chen, J. Y., M. Taniguchi, G. Liu, K. Miyaoka, S.-I. Onodera, T. Tokunaga, and Y. Fukushima (2007), Nitrate pollution of groundwater in the Yellow River delta, China, *Hydrogeology*, *15*(8), 1605–1614, doi:10.1007/s10040-007-0196-7.

Dulaiova, H., and W. C. Burnett (2004), An efficient method for γ-spectrometric determination of radium-226,228 via manganese fibers, *Limnol. Oceanogr. Methods*, *2*(1), 256–261.

Dulaiova, H., W. C. Burnett, G. Wattayakorn, and P. Sojisuporn (2006), Are groundwater inputs into river-dominated areas important? The Chao Phraya River–Gulf of Thailand, *Limnol. Oceanogr. Methods*, *51*(5), 2232–2247.

Hainbucher, D., W. Hao, T. Pohlmann, J. Sündermann, and S. Feng (2004), Variability of the Bohai Sea circulation based on model calcula-

tions, *J. Mar. Syst.*, *44*(3–4), 153–174, doi:10.1016/j.jmarsys.2003.09.008.

Hancock, G. J., I. T. Webster, and T. C. Stieglitz (2006), Horizontal mixing of Great Barrier Reef waters: Offshore diffusivity determined from radium isotope distribution, *J. Geophys. Res.*, *111*, C12019, doi:10.1029/2006JC003608.

Hu, C., F. E. Muller-Karger, and P. Swarzenski (2006), Hurricanes, submarine groundwater discharge, and Florida's red tides, *Geophys. Res. Lett.*, *33*, L11601, doi:10.1029/2005GL025449.

Kim, G., W. C. Burnett, H. Dulaiova, P. Swarzenski, and W. Moore (2001), Measurement of ^{224}Ra and ^{226}Ra activities in natural waters using a radon-in-air monitor, *Environ. Sci. Technol.*, *35*(23), 4680–4683, doi:10.1021/es010804u.

Kim, G., J.-W. Ryu, H.-S. Yang, and S.-T. Yun (2005), Submarine groundwater discharge (SGD) into the Yellow Sea revealed by ^{228}Ra and ^{226}Ra isotopes: Implications for global silicate fluxes, *Earth Planet. Sci. Lett.*, *237*(1–2), 156–166, doi:10.1016/j.epsl.2005.06.011.

Li, Y.-H., and L.-H. Chan (1979), Desorption of Ba and ^{226}Ra from river-borne sediments in the Hudson estuary, *Earth Planet. Sci. Lett.*, *43*(3), 343–350, doi:10.1016/0012-821X(79)90089-X.

MacIntyre, S., R. Wanninkhof, and J. P. Chanton (1995), Trace gas exchange across the air-sea interface in freshwater and coastal marine environments, in *Biogenic Trace Gases: Measuring Emissions from Soil and Water*, edited by P. A. Matson and R. C. Harris, pp. 52–97, Blackwell Sci., Boston, Mass.

Michael, H. A., A. E. Mulligan, and C. F. Harvey (2005), Seasonal oscillations in the water exchange between aquifers and the coastal ocean, *Nature*, *436*(7054), 1145–1148, doi:10.1038/nature03935.

Moore, W. S. (1996), Large groundwater inputs to coastal waters revealed by ^{226}Ra enrichments, *Nature*, *380*(6575), 612–614, doi:10.1038/380612a0.

Moore, W. S. (2000), Ages of continental shelf waters determined from ^{223}Ra and ^{224}Ra, *J. Geophys. Res.*, *105*(C9), 22,117–22,122, doi:10.1029/1999JC000289.

Moore, W. S., and R. Arnold (1996), Measurement of ^{223}Ra and ^{224}Ra in coastal waters using a delayed coincidence counter, *J. Geophys. Res.*, *101*(C1), 1321–1329, doi:10.1029/95JC03139.

Moore, W. S., and J. Krest (2004), Distribution of ^{223}Ra and ^{224}Ra in the plumes of the Mississippi and Atchafalaya rivers and the Gulf of Mexico, *Mar. Chem.*, *86*(3–4), 105–119, doi:10.1016/j.marchem.2003.10.001.

Moore, W. S., and D. F. Reid (1973), Extraction of radium from natural waters using manganese-impregnated acrylic fibers, *J. Geophys. Res.*, *78*(36), 8880–8886, doi:10.1029/JC078i036p08880.

Mulligan, A. E., and M. A. Charette (2006), Intercomparison of submarine groundwater discharge estimates from a sandy unconfined aquifer, *J. Hydrol.*, *327*(3–4), 411–425, doi:10.1016/j.jhydrol.2005.11.056.

Nozaki, Y., Y. Yamamoto, T. Manaka, H. Amakawa, and A. Snidvongs (2001), Dissolved barium and radium isotopes in the Chao Phraya River estuarine mixing zone in Thailand, *Cont. Shelf Res.*, *21*(13–14), 1435–1448, doi:10.1016/S0278-4343(01)00023-1.

Santos, I. R., W. C. Burnett, J. P. Chanton, B. Mwashote, I. G. N. A. Suryaputra, and T. Dittmar (2008), Nutrient biogeochemistry in a Gulf of Mexico subterranean estuary and groundwater-derived fluxes to the coastal ocean, *Limnol. Oceanogr. Methods*, *53*(2), 705–718.

Slomp, C. P., and P. Van Cappellen (2004), Nutrient inputs to the coastal ocean through submarine groundwater discharge: Controls and potential impact, *J. Hydrol.*, *295*(1–4), 64–86, doi:10.1016/j.jhydrol.2004.02.018.

Spiteri, C., C. P. Slomp, K. Tuncay, and C. Meile (2008), Modeling biogeochemical processes in subterranean estuaries: Effect of flow dynamics and redox conditions on submarine groundwater discharge of nutrients, *Water Resour. Res.*, *44*, W02430, doi:10.1029/2007WR006071.

Swarzenski, P. W., C. Reich, K. D. Kroeger, and M. Baskaran (2007a), Ra and Rn isotopes as natural tracers of submarine groundwater discharge in Tampa Bay, FL, *Mar. Chem.*, *104*(1–2), 69–84.

Swarzenski, P. W., F. W. Simonds, A. J. Paulson, S. Kruse, and C. Reich (2007b), Geochemical and geophysical examination of submarine groundwater and associated nutrient loading estimates into Lynch Cove, Hood Canal, WA, *Environ. Sci. Technol.*, *41*(20), 7022–7029, doi:10.1021/es070881a.

Taniguchi, M., and T. Iwakawa (2001), Measurements of submarine groundwater discharge rates by a continuous heat - type automated seepage meter in Osaka Bay, Japan, *J. Groundwater Hydrol.*, *42*, 271–277.

Taniguchi, M., T. Ishitobi, J. Chen, S.-I. Onodera, K. Miyaoka, W. C. Burnett, R. Peterson, G. Liu, and Y. Fukushima (2008), Submarine groundwater discharge from the Yellow River delta to the Bohai Sea, China, *J. Geophys. Res.*, *113*, C06025, doi:10.1029/2007JC004498.

Wang, Q., X. Guo, and T. Kidetaka (2007), A numerical study on the seasonal variation of Yellow River plume path in the Bohai Sea, paper presented at 3rd International Workshop on Yellow River Studies, Res. Inst. for Humanity and Nat., Kyoto, Japan.

Yu, L. (2006), The Huanghe (Yellow) River: Recent changes and its countermeasures, *Cont. Shelf Res.*, *26*(17–18), 2281–2298, doi:10.1016/j.csr.2006.07.026.

Zhang, J., Z. G. Yu, T. Raabe, S. M. Liu, A. Starke, L. Zou, H. W. Gao, and U. Brockmann (2004), Dynamics of inorganic nutrient species in the Bohai seawaters, *J. Mar. Syst.*, *44*(3–4), 189–212, doi:10.1016/j.jmarsys.2003.09.010.

W. C. Burnett, R. N. Peterson, and I. R. Santos, Department of Oceanography, Florida State University, Tallahassee, FL 32306-4320, USA. (wburnett@fsu.edu; peterson@ocean.fsu.edu; santos@ocean.fsu.edu)

J. Chen, School of Geography Sciences and Planning, Sun Yat-sen University, Xingang West Road 135, Guangzhou 510275, China. (chenjyao@mail.sysu.edu.cn)

T. Ishitobi and M. Taniguchi, Research Institute for Humanity and Nature, 335 Takashima-cho, Kamigyo-ku, Kyoto 602-0878, Japan. (tomotoshi@chikyu.ac.jp; makoto@chikyu.ac.jp)